Direct test of defect-mediated laser-induced melting theory for two-dimensional solids

Debasish Chaudhuri* and Surajit Sengupta†
Satyendra Nath Bose National Centre for Basic Sciences, Block-JD, Sector-III, Salt Lake, Calcutta 700098, India
(Received 16 August 2005; revised manuscript received 2 December 2005; published 30 January 2006)

We investigate by direct numerical solution of appropriate renormalization flow equations the validity of a recent dislocation unbinding theory for laser-induced freezing and melting in two dimensions. The bare elastic moduli and dislocation fugacities are obtained for three different two-dimensional systems namely, the hard disk, inverse 12th power, and Derjaguin-Landau-Verwey-Overbeek potentials. A restricted Monte Carlo simulation sampling only configurations without dislocations is used to obtain these quantities. These are then used as inputs to the flow equations. Numerical solution of the flow equations then yields the phase diagrams. We conclude that (a) the flow equations need to be correct at least up to third order in defect fugacity to reproduce meaningful results, (b) there is excellent quantitative agreement between our results and earlier conventional Monte Carlo simulations for the hard disk system, and (c) while the qualitative form of the phase diagram is reproduced for systems with soft potentials there is some quantitative discrepancy which we explain.

DOI: 10.1103/PhysRevE.73.011507 PACS number(s): 64.70.Dv, 64.60.Ak, 82.70.Dd

I. INTRODUCTION

Examples of phase transitions mediated by the unbinding of defect pairs abound in two dimensions. The quasi-long-ranged order to disorder transition in the *XY* and planar rotor models [1–6], the melting transition of two-dimensional solids [1,7–11], the superconductor to normal phase transition in two-dimensional Josephson junction arrays [12], the commensurate-incommensurate transition of the striped phase of smectic liquid crystals on anisotropic substrates [13], and the more recent discovery of a defect-mediated reentrant freezing transition in two-dimensional colloids in an external periodic potential [14,15] are all understood within such defect unbinding theories. While the very first defect-mediated transition theory for the phase transition in the *XY* model by Kosterlitz and Thouless (KT) [1] enjoyed almost immediate acceptance and was verified in simulations [2–4,6] as well as experiments [16,17], defect-mediated theories of two-dimensional melting took a long time to gain general acceptance in the community [18]. There were several valid reasons for this reticence however.

First, as was recognized even in the earliest papers [8,9] on this subject, the dislocation unbinding transition, which represents an instability of the solid phase, may always be pre-empted by a first-order [19,20] transition from a metastable solid to a stable liquid. Whether such a first-order melting transition actually occurs or not depends on the temperature of instability T_{KT}; so that if the transition temperature $T_c < T_{KT}$ the unbinding of dislocations does not occur. Clearly, neither this condition nor its converse can hold for all two-dimensional (2D) systems in general. This is because T_{KT} is a nonuniversal number which depends on the "distance" in coupling parameter space between the bare and the fixed point Hamiltonians and hence on the details of the interaction. Second, the renormalization group (RG) flow equations derived in all defect-mediated theories to date are perturbative expansions in the defect density (fugacity) in the ordered phase. How fast does this perturbation series converge? The answer lies again in the position of the bare Hamiltonian in the coupling parameter space. For the planar rotor model [1,6], past calculations show that next to leading order terms in the flow equations are essential to reproduce the value of the transition temperature obtained in simulations [6]. Third, defect-mediated transitions predict an essential singularity [1] of the correlation length at the transition temperature. This means that effects of finite size [21] would be substantial and may thoroughly mask the true thermodynamic result. A rapid increase of the correlation length also implies that the relaxation time diverges as the transition temperature is approached—critical slowing down. For the two-dimensional solid, this last effect is particularly crucial since, even far from the transition, the motion of defects is mainly thermally assisted and diffusional and therefore slow. The equilibration of defect configurations [22] is therefore often an issue even in solids of macroscopic dimensions.

On the other hand, over the last few years it has been possible to test quantitatively some of the nonuniversal predictions of defect-mediated theories of phase transitions using simulations of restricted systems [6,11,23]. A simulation of a system without defects is used to obtain the values for the bare coupling constants which are then taken as inputs to the renormalization group equations for the appropriate defect unbinding theory to obtain quantities like the transition temperature. Needless to say, the simulated system does not undergo a phase transition and therefore problems typically related to diverging correlation lengths and times do not occur. Numerical agreement of the result of this calculation with that of unrestricted simulations or experiments is proof of the validity of the RG flow equations [1,8,9,11]. This idea has been repeatedly applied in the past to analyze defect-mediated phase transitions in the planar rotor model [6], two-dimensional melting of hard disks [11], and the reentrant freezing of hard disks in an external periodic potential [23,24]. The last system is particularly interesting in view of its close relation with experiments on the laser-induced reen-

*Electronic address: debc@bose.res.in
†Electronic address: surajit@bose.res.in

trant freezing transition in charge-stabilized colloids [14,15] and this constitutes the subject of the present paper as well.

In this paper we show in detail how restricted simulations of systems of particles interacting among themselves via a variety of interactions and with a commensurate external periodic potential can be used to obtain phase diagrams showing the reentrant freezing transition. The results obtained are compared to earlier unrestricted simulations for the same systems. Briefly our results are as follows. First, we observe that, as in an earlier study of the planar rotor model [6], next to leading order corrections to the renormalization flow equations are *essential* to reproduce even the gross features of the phase diagram. Specifically, the reentrant portion of the phase diagram can be reproduced *only* if such correction terms are taken into account. Second, while we find almost complete agreement with earlier results for the hard disk system which has been studied most extensively, our phase diagram for the other forms of interaction is shifted with respect to the results available in the literature. This may mean either of two things—inadequacy of the RG theory used by us or finite size effects in the earlier results. Last, as a by-product of our calculations, we have obtained the core energy for defects (dislocations) in these systems and studied its dependence on thermodynamic and potential parameters.

The problem of reentrant freezing transition of a system of interacting colloidal particles in a periodic potential has an interesting history involving experiments [14,15], simulations [25–33], and theory [34–36]. In the last couple of decades soft systems like colloids have been studied extensively [37] both for their own sake and as typical toy models to study various important condensed matter questions like structural and phase transitions through experiments that allow real space imaging. Charged colloids confined within two glass plates form a model 2D system as the electrostatic force from the plates almost completely suppresses the fluctuations of colloids perpendicular to the plates, practically confining them to a 2D plane. In their pioneering experiment Chowdhury *et al.* [14] imposed a simple static background potential which is periodic in one direction and constant in the other (except for an overall Gaussian profile of intensity variation) by interfering two laser beams. This potential immediately induces a density modulation in the colloidal system. The potential minima are spaced to overlap with the close packed lines of the ideal lattice of the colloidal system at a given density. With increase in potential strength such a colloidal liquid has been observed to solidify. This is known as laser-induced freezing (LIF). In a recent experiment [15] it has been shown that with further increase in potential strength, surprisingly, the solid phase remelts into a modulated liquid. This phenomenon is known as reentrant laser-induced freezing (RLIF). Qualitatively, starting from a liquid phase, the external periodic potential immediately induces a density modulation, reducing fluctuations which eventually leads to solidification. Further increase in the amplitude of the potential reduces the system to a collection of decoupled 1D strips. The dimensional reduction now *increases* fluctuations remelting the system.

The early mean field theories, namely, Landau theory [14] and density functional theory [34], predicted a change from a first-order to a continuous transition with increase in potential strength and failed to describe the reentrant behavior, a conclusion seemingly confirmed by early experiments [14] and some early simulations [25]. Overall, the results from early simulations remained inconclusive however; while one of them [25] claimed to have found a tricritical point at intermediate laser intensities and reentrance, later studies refuted these results [26–28]. All of these studies used the change in order parameter and the maximum in the specific heat to identify the phase transition points. While some later studies [26–28] found RLIF for hard disks they reported laser-induced freezing and absence of any reentrant melting for the Derjaguin-Landau-Verwey-Overbeek (DLVO) potential [28] in direct contradiction to experiments [15].

Following the defect-mediated disordering approach of Kosterlitz and Thouless [1], Frey, Nelson, and Radzihovsky (FNR) [35] proposed a detailed theory for the reentrant transition based on the unbinding of dislocations with Burgers vector parallel to the line of potential minima. This theory predicted RLIF and no tricritical point. The results of this work were in qualitative agreement with experiments [15] and provided a framework for understanding RLIF in general. More accurate simulation studies on systems of hard disks [29], soft disks [31,32], DLVO potential [30], etc., confirmed the reentrant freezing-melting transition in agreement with experiments [15] and FNR theory [35,36]. In these studies the phase transition point was found from the crossing of Binder cumulants [38,39] of order parameters corresponding to translational and bond-orientational order, calculated for various subsystem sizes. A systematic finite size scaling analysis [29] of simulation results for the 2D hard disk system in a 1D modulating potential showed, in fact, several universal features consistent with the predictions of FNR theory. It was shown in these studies that the resultant phase diagram remains system size dependent and the crossover to the zero-field Kosterlitz-Thouless-Halperin-Nelson-Young (KTHNY) melting [8,9] plays a crucial role in understanding the results for small values of the external potential. While the data collapse and critical exponents were consistent with KT theory for stronger potentials, for weaker potentials they match better with critical scaling [29]. A common problem with all the simulation studies might be equilibration with respect to dislocation movements along climb (or even glide) directions. Also, nonuniversal predictions, namely, the phase diagram are difficult to compare because the FNR approach (like KT theory) is expressed in terms of the appropriate elastic moduli which are notoriously time-consuming to compute near a continuous phase transition. Diverging correlation lengths and times near the phase transition further complicate an accurate evaluation of the nonuniversal predictions of the theory.

We calculate the phase diagrams of three different 2D systems with a 1D modulating potential (see Fig. 1) following the technique of restricted Monte Carlo simulations [6,11,23], to be discussed below. For the laser-induced transition we use this method to generate whole phase diagrams. We reject Monte Carlo moves which tend to distort a unit cell in a way that changes the local connectivity [11]. The percentage of moves thus rejected is a measure of the dislocation fugacity [11]. This, together with the elastic constants of the dislocation free lattice obtained separately, are our

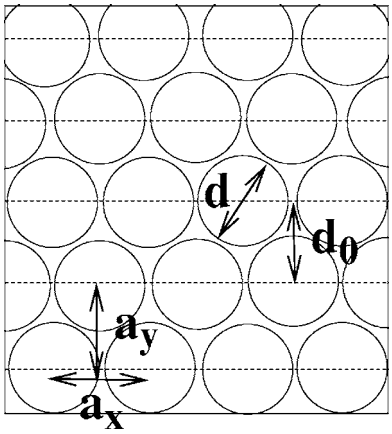

FIG. 1. This cartoon shows a typical 2D system under consideration. d is the length scale over which repulsive two-body potentials are operative. The dashed lines indicate minima of external modulating potential $\beta V(y) = -\beta V_0 \cos(2\pi y/d_0)$. $a_x = a_0$ is the lattice parameter fixed by the density ρ and a_y indicate the average separation between two layers along the y direction perpendicular to a set of close-packed planes. For a perfect triangular lattice $a_y = \sqrt{3}a_0/2$. The modulating potential is commensurate with the lattice such that $d_0 = a_y$.

inputs (bare values) to the renormalization flow equations [35,36] to compute the melting points and hence the phase diagram. Our results (Figs. 13, 16, and 17) clearly show a modulated liquid (ML) → locked floating solid (LFS) → ML reentrant transition with increase in the amplitude (V_0) of the potential. In general, we find the predictions of FNR theory to be valid.

Last, we must mention that our technique, as summarized above and used in this as well as earlier work [23], corresponds closely with early studies of the melting of the electron solid by Morf [7,40]. In the latter case, the dislocation fugacity, which is one of the important inputs to the KTHNY flow equations, was obtained by a careful and direct calculation of the dislocation core energy at $T=0$. Our approach is somewhat cruder but gives us numbers for nonzero T which automatically contain the effects of phonon fluctuations.

In Sec. II we first briefly discuss the FNR theory and then go on to show in detail the restricted simulation scheme used by us to obtain the various quantities required to calculate the phase diagram. In Sec. III we give the simulation results. We describe, in detail, the various quantities leading to the phase diagram for one of the systems, viz., the hard disks [11,41]. Then we present the phase diagrams for the other two systems we study. We compare our results with earlier simulations. Last, in Sec. IV we summarize our main results and conclude.

II. METHOD

A cartoon corresponding to the systems considered for our study is given in Fig. 1. The elastic free energy of the solid is given in terms of the spatial derivatives of the displacement field $\vec{u}(\vec{r}) = \vec{r} - \vec{r}_0$ with $\vec{r}_0$ being the lattice vectors of the undistorted reference triangular lattice. For a solid in presence of a modulating potential $\beta V(y)$ (Fig. 1) the displacement mode u_y becomes massive, leaving massless u_x modes. After integrating out the u_y modes the free energy of the LFS may be expressed in terms of gradients of u_x and elastic moduli [35,36], namely, the Young's modulus $K(\beta V_0, \rho)$ and shear modulus $\mu(\beta V_0, \rho)$,

$$\mathcal{H}_{el} = \int dx\, dy \left[\frac{1}{2} K \left(\frac{\partial u_x}{\partial x} \right)^2 + \frac{1}{2} \mu \left(\frac{\partial u_x}{\partial y} \right)^2 \right]. \tag{1}$$

Similar arguments [35,36] show that among the three sets of low-energy dislocations available in the 2D triangular lattice, only those (type I) with Burgers vector parallel to the line of potential minima survive at large βV_0. Dislocations with Burgers vector pointing along the other two possible close-packed directions (type II) in the 2D triangular lattice have larger energies because the surrounding atoms are forced to ride the crests of the periodic potential [35,36]. Within this set of assumptions, the system therefore shares the same symmetries as the XY model. Indeed, a simple rescaling of $x \to \sqrt{\mu}x$ and $y \to \sqrt{K}y$ leads this free energy to the free energy of the XY model with spin-wave stiffness $K_{xy} = \sqrt{K\mu}a_0^2/4\pi^2$ and spin angle $\theta = 2\pi u_x/a_0$:

$$\mathcal{H}_{el} = \int dx\, dy \left(\frac{1}{2} K_{xy} (\nabla \theta)^2 \right).$$

This immediately leads to the identification of a vortex in XY model ($\oint d\theta = 2\pi$) with a dislocation of Burgers vector $\vec{b} = \hat{i}a_0$ ($\oint du_x = a_0$, $\hat{i}$ = unit vector along x direction) parallel to the potential minima, i.e., the dislocation of type I. The corresponding theory for phase transitions can then be recast as a KT theory [1] and is described in the framework of a two-parameter renormalization flow for the spin-wave stiffness $\beta K_{xy}(l)$ and the fugacity of type I dislocations $y'(l)$, where l is a measure of length scale as $l = \ln(r/a_0)$, r being the size of the system. The flow equations are expressed in terms of $x' = (\pi \tilde{K}_{xy} - 2)$ where $\tilde{K}_{xy} = \beta K_{xy}$ and $y' = 4\pi \exp(-\beta E_c)$ where E_c is the core energy of type I dislocations which is obtained from the dislocation probability [11,40]. Keeping up to next to leading order terms in y' the renormalization group flow equations [6,42] are

$$\frac{dx'}{dl} = -y'^2 - y'^2 x',$$

$$\frac{dy'}{dl} = -x'y' + \frac{5}{4} y'^3. \tag{2}$$

Flows in l generated by the above equations starting from initial or "bare" values of x' and y' fall in two categories. If, as $l \to \infty$, y' diverges, the thermodynamic phase is disordered (i.e., ML), while on the other hand if y' vanishes, it is an ordered phase (a LFS) [35,36]. The two kinds of flows are demarcated by the *separatrix* which marks the phase transition point. For the linearized equations, which keep only the leading order terms in y', the separatrix is simply the straight line $y' = x'$, whereas for the full nonlinear equations one needs to calculate this numerically [6,11,42].

The bare numbers for x' and y' are relatively insensitive to system size since our Monte Carlo (MC) simulation does not involve a diverging correlation length associated with a phase transition. This is achieved as follows [6,11]. We monitor individual random moves of the particles in a system and look for distortions of the neighboring unit cells. If in any of these unit cells the length of a next nearest neighbor bond becomes smaller than the nearest neighbor bond, the move is rejected. All such moves generate disclination quartets and are shown in Fig. 2. Notice that each of these moves break a nearest neighbor bond to build a new next nearest neighbor bond, in the process generating two 7-5 disclination pairs. These are the moves rejected in the restricted simulation scheme we follow. The probabilities of such bond breaking moves are, however, computed by keeping track of the number of such rejected moves. One has to keep track of all the three possible distortions of the unit rhombus with measured probabilities P_{mi}, $i=1, 2, 3$ (see Fig. 2),

$$P_{mi} = \frac{\text{number of rejected bond breaking moves of type } i}{\text{total number of MC moves}}.$$

Each of these distortions involves four 7-5 disclinations, i.e., two possible dislocation-antidislocation pairs which, we assume, occur mutually exclusively in a way that we explain shortly. For a free ($V_0=0$) two-dimensional system the dislocation core energy E_c^t can be found through the relation [40]

$$\Pi = \exp(-\beta 2E_c^t) Z(\tilde{K}) \tag{3}$$

where $\Pi=\Sigma_{i=1}^{3} P_{mi}$ is the total number density of dislocation pairs per particle and $Z(\tilde{K})$ is the "internal partition function" incorporating all three types of degenerate orientations of dislocations,

$$Z(\tilde{K}) = \frac{2\pi\sqrt{3}}{\tilde{K}/8\pi - 1}\left(\frac{r_{min}}{a_0}\right)^{2-\tilde{K}/4\pi} I_0\left(\frac{\tilde{K}}{8\pi}\right)\exp\left(\frac{\tilde{K}}{8\pi}\right),$$

where I_0 is a modified Bessel function, $\tilde{K}=\beta K a_0^2$ is a dimensionless Young's modulus renormalized over phonon modes, a_0 being the lattice parameter and r_{min} is the separation between dislocation and antidislocation above which one counts the pairs. The above expression for $Z(\tilde{K})$ and Eq. (3) have been used previously in simulations [11,40] of phase transitions of 2D systems in absence of any external potential to find the dislocation core energy E_c^t.

We now show how the probabilities for generating pairs of specific types of dislocations P_{di} for $V_0 \neq 0$ are related to P_{mi}. Consider Fig. 2 where each of the three varieties of bond breaking moves are depicted. It is clear that each given distortion can occur due to the presence of two possible dislocation-antidislocation pairs acting independently. For example, a distortion of type A can take place either due to dislocation dipoles with Burgers vectors making an angle of 60° with the horizontal or an angle of 120°. Both of these dislocation dipoles are of type II. If this bond breaking move were to be accepted, then at a subsequent time step the individual dislocations making up any one of the two possible

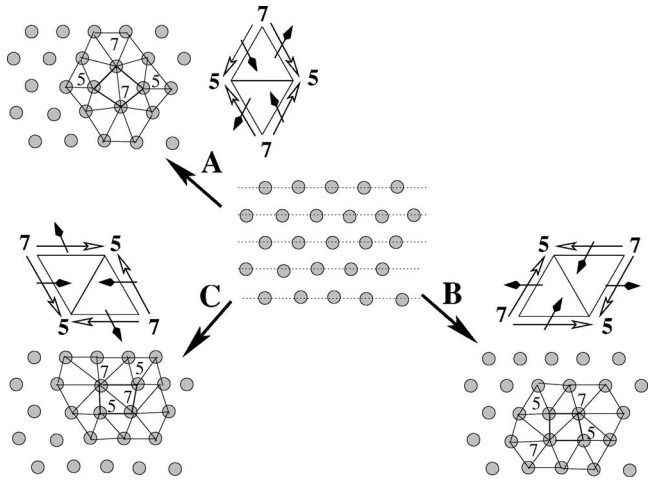

FIG. 2. This diagram depicts all the possible dislocation generating moves that we reject. Starting from the triangular lattice shown in the center (the dotted lines show the potential minima), in all, there can be three types of dislocation-pair generating moves shown as A, B, and C. The numbers 7 and 5 denote the positions of two types of disclinations having seven nearest neighbors and five nearest neighbors, respectively. Only those bonds that, are necessary to show distortions due to the generation of disclination quartets have been drawn. The rhombi near each of the distorted lattices denote the unit cells and open arrows from $7 \rightarrow 5$ show the direction of dislocation-generating moves. The probabilities of these moves are P_{m1} (A), P_{m2} (B), and P_{m3} (C). Corresponding Burgers vectors (filled arrows) are bisectors pointing toward a direction rotated counterclockwise starting from $7 \rightarrow 5$ directions and are parallel to one of the lattice planes. Notice that the separation between Burgers vectors of a pair along the glide direction (parallel to the Burgers vectors) is a single lattice separation (a_0) and within this construction it is impossible to draw a Burgers loop that can generate a nonzero Burgers vector. Depending on which of the two possible disclination pairs separates out any one dislocation-antidislocation pair will be formed.

pairs could separate, the two possible events being mutually exclusive. This allows us to write down the following relations among the various probabilities:

$$P_{m1} = P_{d2} + P_{d3}, \quad P_{m2} = P_{d2} + P_{d1}, \quad P_{m3} = P_{d3} + P_{d1}.$$

Solving for P_{di}s and remembering that $P_{d2}=P_{d3}$ by symmetry, we get $P_{d1}=\frac{1}{2}(P_{m2}+P_{m3}-P_{m1})$ and $P_{d2}=P_{m1}/2$. The above expressions are motivated and illustrated in Fig. 2. Once the probability of dislocation pairs is obtained in this fashion, we may proceed to calculate the dislocation core energy E_c and the dislocation fugacity y'.

An argument following the lines of Fisher *et al.* [40] shows that the dislocation probability (number density of dislocation pair per particle) for our system,

$$P_{d1} = \exp(-\beta 2E_c) Z(\tilde{K}_{xy}), \tag{4}$$

where $2E_c$ is the core energy and $Z(\tilde{K}_{xy})$ is the internal partition function of dislocation pairs of type I (single orientation):

$$Z(\tilde{K}_{xy}) = \int_{r>r_{min}} \frac{d^2r}{A_c} \exp\left[-2\pi\tilde{K}_{xy}\ln\left(\frac{r}{a_0}\right)\right] = \frac{2\pi}{\sqrt{3}} \frac{(r_{min}/a_0)^{2-2\pi\tilde{K}_{xy}}}{\pi\tilde{K}_{xy}-1} \quad (5)$$

with $\tilde{K}_{xy}=\beta K_{xy}$ and $A_c=\sqrt{3}a_0^2/2$ being the area of a unit cell in the undistorted lattice. We choose $r_{min}=2a_0$. At this point this choice is arbitrary. We give the detailed reasoning for this choice at the end of the discussions on hard disks in Sec. III. Equations (4) and (5) straightaway yield the required core energy E_c. The corresponding fugacity contribution to RG flow equations [Eq. (2)] is given via

$$y' = 4\pi\sqrt{P_{d1}/Z(\tilde{K}_{xy})}. \quad (6)$$

In the above, the following assumption is, however, implicit. Once a nearest neighbor bond breaks and a potential dislocation pair is formed, they separate with probability 1 [43]. This assumption goes into the identity Eq. (4) as well as into Eq. (3) [11]. Taking the rejection ratios due to bond breaking as the dislocation probabilities, as well, requires this assumption [44].

The same restricted Monte Carlo simulation can be used to find the stress tensor and the elastic moduli from the stress-strain curves. The dimensionless stress tensor for a free ($V_0=0$) system is given by [45]

$$\beta\sigma_{\lambda\nu}d^2 = -\frac{d^2}{S}\left(-\sum_{\langle ij\rangle}\left\langle \beta\frac{\partial\phi}{\partial r^{ij}}\frac{r_\lambda^{ij}r_\nu^{ij}}{r^{ij}}\right\rangle + N\delta_{\lambda\nu}\right) \quad (7)$$

where i,j are particle indices and λ,ν denote directions x,y; $\phi(r^{ij})$ is the two-body interaction, and S/d^2 is the dimensionless area of the simulation box [46].

III. RESULTS AND DISCUSSION

In this section we present the results from our simulations for three different 2D systems, namely, hard disks, soft disks, and a system of colloidal particles interacting via the DLVO [47,48] potentials. We discuss, first, our calculation for a two-dimensional system of hard disks, in detail. The procedure followed in other systems is almost identical.

A. Hard disks

The bulk system of hard disks where particles i and j, in 2D, interact via the potential $\phi(r^{ij})=0$ for $r^{ij}>d$ and $\phi(r^{ij})=\infty$ for $r^{ij}\leq d$, where d is the hard disk diameter and $r^{ij}=|\mathbf{r}^j-\mathbf{r}^i|$ the relative separation of the particles, is known to melt [11,41,49–51] from a high-density triangular lattice to an isotropic liquid with a narrow intervening hexatic phase [8,9,11,41]. The hard disk free energy is entirely entropic in origin and the only thermodynamically relevant variable is the number density $\rho=N/V$ or the packing fraction $\eta=(\pi/4)\rho d^2$. Simulations [41], and experimental [37] and theoretical [52] studies of hard disks show that for $\eta>0.715$ the system exists as a triangular lattice which transforms to a liquid below $\eta=0.706$. The small intervening region contains a hexatic phase predicted by the KTHNY theory [8,9] of 2D melting. Apart from being easily accessible to theoretical treatment [53], experimental systems with nearly "hard" interactions, viz., sterically stabilized colloids [37], are available.

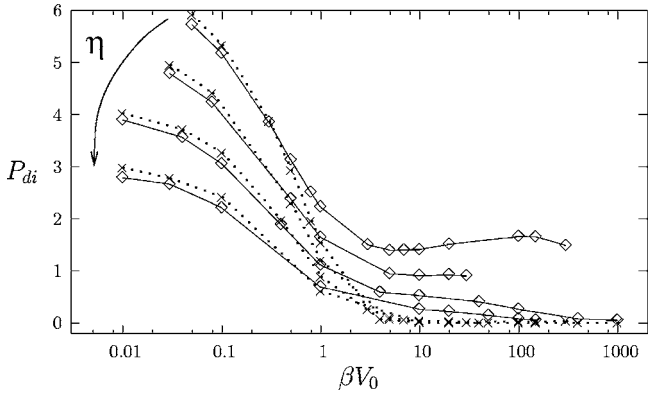

FIG. 3. Number density of dislocation pairs of types I and II per particle as a function of the amplitude of the laser potential βV_0. In this plot the ◇ symbols correspond to P_{d1}, the probability for type I dislocations, and the × symbols to P_{d2}, the probability for type II dislocations obtained from the P_{mi} (see text and Fig. 2) for various η values, arrow denoting the direction of increasing η (=0.69, 0.696, 0.7029, 0.71). The P_{di} for $i=1$, 2 are multiplied by 10^4. These probabilities are plotted against the potential strength βV_0. Note that for $\beta V_0>1$, the probability for type I dislocations is larger than that of type II. The dots and solid lines are only guides to the eye.

In the presence of a periodic external potential, the only other energy scale present in the system is the relative potential [54] strength βV_0. If the modulating potential is commensurate with the spacing between close-packed lines, the elastic free energy of this system in its solid phase follows Eq. (1) and the corresponding renormalization flow equations are given by Eq. (2).

We obtain the bare y' and x' from Monte Carlo simulations of $43\times 50=2150$ hard disks and use them as initial values for the numerical solution of Eqs. (2). The Monte Carlo simulations for hard disks is done in the usual [55] way, viz., we perform individual random moves of hard disks after checking for overlaps with neighbors. When a move is about to be accepted, however, we look for the possibility of bond breaking as described in the previous section (Fig. 2). We reject any such move and the rejection ratios for specific types of bond breaking moves give us the dislocation probabilities of type I and II, separately (Fig. 3).

From Fig. 3 it is clear that the probability of type II dislocations, i.e., P_{d2}, drops down to zero for all packing fractions at higher potential strengths βV_0. The external potential suppresses formation of this kind of dislocations. For small βV_0, on the other hand, the probabilities of type I and type II dislocations are roughly the same. This should be a cause of concern since we neglect the contribution of type II dislocations for *all* βV_0. We comment on this issue later in this section. Using Eqs. (5) and (6) along with the identity $r_{min}=2a_0$ gives us the initial value y_0' to be used in renormalization flow Eq. (2).

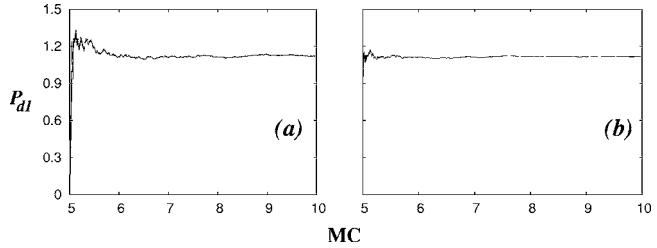

FIG. 4. P_{d1} as a function of MC steps. P_{d1} has been multiplied by 10^4 and number of MC steps has been multiplied by 10^{-4} for clarity. The data have been collected for $\eta=0.7029$ and $\beta V_0=1$. (a) is for system size of 2150 particles whereas (b) is for 21 488 particles. Within 10^5 MC steps all fluctuations die out. Clearly, the dependence of the dislocation number density on the system sizes and the Monte Carlo errors is negligible. To calculate dislocation fugacity we use averaging of data between 5×10^5 and 10^6 MC steps.

Before we move on, we comment on the magnitude of the errors for P_{mi} and hence for y_0'. There are two main sources of errors for these quantities. They may arise from (a) finite simulation times and (b) the small size of the system. In order to check for this, we have plotted the accumulated values for the probability P_{d1} as a function of Monte Carlo step for 2150 and 21 488 hard disks (Fig. 4). It is clear that our estimates for the probabilities are virtually error free! This demonstrates clearly the usefulness of our restricted Monte Carlo scheme. To obtain K_{xy} we need to calculate the Young's modulus K and shear modulus μ. In order to do that consider Eq. (7), the expression for the stress tensor. For hard disk potentials the derivative $\partial\phi/\partial r^{ij}$ becomes a Dirac δ function and the expression for stress can be recast into [45]

$$\beta\sigma_{\lambda\nu}d^2 = -\frac{d^2}{S}\left(\sum_{\langle i,j\rangle}\left\langle \frac{r_\lambda^{ij}r_\nu^{ij}}{r^{ij}}\delta(r^{ij}-d)\right\rangle + N\delta_{\lambda\nu}\right). \qquad (8)$$

The presence of the Dirac delta function $\delta(r^{ij}-d)$ in the above expression requires that the terms under the summation contribute, strictly, when two hard disks touch each other, i.e., $r^{ij}\equiv r=\sigma$. In practice, we implement this, by adding the terms under summation when each pair of hard disks comes within a small separation $r=\sigma+\delta$. We then find $\beta\sigma_{\lambda\nu}d^2$ as function of δ and fit the curve to a second-order polynomial. Extrapolating to the $\delta\to0$ limit obtains the value of a given component of stress tensor at each strain value $\epsilon_{\lambda\nu}$ [45] (Figs. 5 and 6).

For completeness, now we show how we calculate the two relevant elastic moduli from the stresses : σ_{xx} at a given longitudinal strain ϵ_{xx} (Fig. 5) and σ_{xy} for a shear strain ϵ_{xy} (Fig. 6). All the data points are from our MC simulations averaged between 10 000 and 20 000 MC steps. Increasing the number of configurations does not change the values significantly. The total errors arising from the MC simulations and the fit for a typical calculation of stresses is less than a percent. We thus calculate the stress at each value of strain and from the slopes of stress-strain curves find out the bare Young's modulus βKd^2 (Fig. 7) and shear modulus $\beta\mu d^2$ (Fig. 8). We impose an elongational strain in the x direction which is parallel to the direction of potential minima to obtain βKd^2. Imposition of a shear strain in the same direction gives us $\beta\mu d^2$. Any strain that forces the system to ride potential hills will give rise to massive displacement modes which do not contribute to elastic theory. Our results for the stress strain curves for obtaining βKd^2 and $\beta\mu d^2$ are shown in Figs. 6 and 8, respectively. Note that the errors for the calculation of the elastic constants arise solely from the fitting of the stress-strain curves. These can be made as small as possible by increasing the number of strain values at which the stresses are calculated. The values of the stress are also free from any residual finite size effects which we checked by simulating systems of sizes 10×10 to 136×158. From these elastic moduli we get the "bare" $\tilde{K}_{xy}$ (and hence $x_0'=\pi\tilde{K}_{xy}-2$; see Sec. II). Our final estimates for the bare $\tilde{K}_{xy}$ are also correct to within 1%.

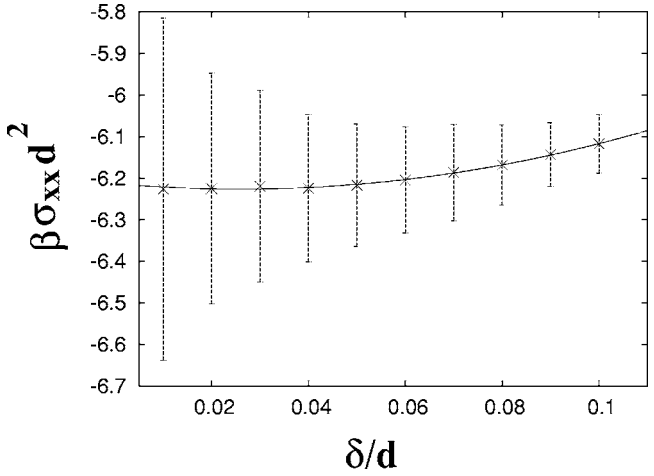

FIG. 5. Plot of $\beta d^2\sigma_{xx}$ vs δ/d at a strain value $\epsilon_{xx}=0.02$ for packing fraction $\eta=0.7029$ and potential strength $V_0=1$. A second-order polynomial fit (solid line) utilizing the error bars to assign weights to each data point gives $\lim_{\delta\to0}\beta d^2\sigma_{xx}=-6.21$ with an error within 0.08%.

In Ref. [36] it is argued that the elastic constant βKd^2 remains more or less independent of amplitude of the laser

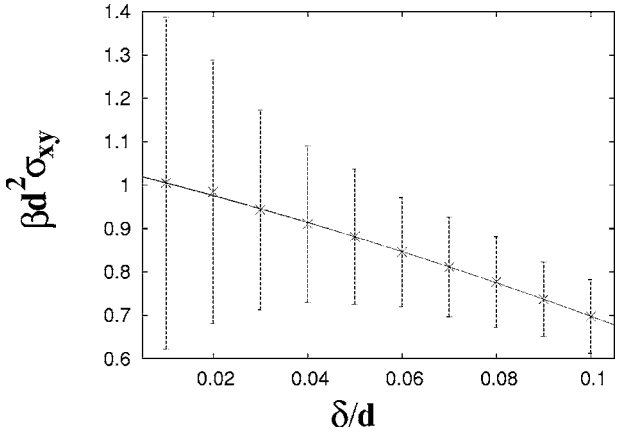

FIG. 6. Plot of $\beta d^2\sigma_{xy}$ vs δ/d at strain value $\epsilon_{xy}=0.079$ at the packing fraction $\eta=0.7029$ and potential strength $V_0=1$. A second-order polynomial fit (solid line) gives $\lim_{\delta\to0}\beta d^2\sigma_{xy}=1.033$ with an error within 0.5%.

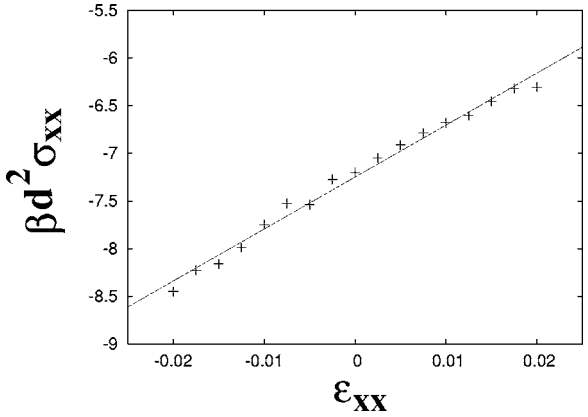

FIG. 7. A typical stress-strain curve used to obtain the Young's modulus from a linear fit (solid line). The graph is plotted at $\eta=0.7029$, $V_0=1.0$. The fitted Young's modulus $\beta Kd^2=54.5$ with an error within 2.9%. The error bars in stress are less than 0.2% and much smaller than the point sizes plotted in this graph.

potential βV_0, while the shear modulus decreases linearly with increasing βV_0 for large βV_0. In Figs. 9 and 10 we have plotted the values of βKd^2 and $\beta\mu d^2$, respectively, as a function of βV_0. It is apparent that the expectations of Ref. [36] are borne out by our data. Incidentally, the behavior of βKd^2 and $\beta\mu d^2$ with increasing βV_0 offers an intuitive interpretation of the RLIF transition which we offer below.

In Fig. 11 we have plotted x_0' and y_0', the bare values of x' and y' for various potential strengths βV_0, at packing fraction $\eta=0.7029$ along with the separatrices for the linearized and the nonlinear flow equations [Eq. (2)]. The line of initial conditions is seen to cross the nonlinear separatrix twice (signifying reentrant behavior) while crossing the corresponding linearized separatrix only once at high potential strengths. For small βV_0 the freezing transition is seen to be driven mainly by the decrease of y' (the dislocation density) since βKd^2 and $\beta\mu d^2$ are virtually constant. For large βV_0, the shear modulus $\beta\mu d^2$ vanishes and this results in the second point of intersection with the separatrix (remelting). The

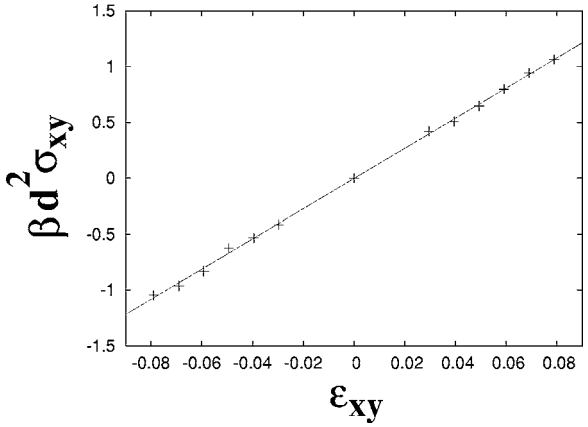

FIG. 8. A typical stress-strain curve used to obtain shear modulus from a linear fit (solid line). The graph is plotted at $\eta=0.7029$, $V_0=1.0$. The fitted shear modulus $\beta\mu d^2=13.5$ with an error within 0.9%. The error bars in stress are less than 0.5% and much smaller than the point sizes plotted in this graph.

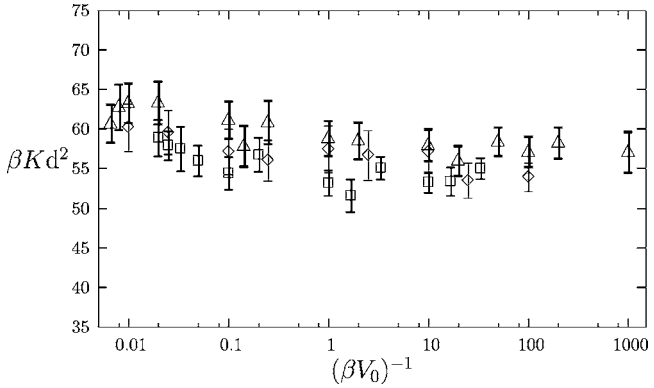

FIG. 9. Young's modulus βKd^2 as a function of inverse laser potential $(\beta V_0)^{-1}$. Various symbols denote different densities: ◇ denotes $\eta=0.7029$, △ denotes $\eta=0.705$, and □ denotes $\eta=0.7$. The data for Figs. 9 and 10 were obtained from a separate run with a slightly higher error than that in Figs. 7 and 8.

phase diagram (Fig. 12) is obtained by computing the points at which the line of initial conditions cut the nonlinear separatrix using a simple interpolation scheme. It is interesting to note that within a linear theory the KT flow equations *fail to predict a RLIF transition*. Performing the same calculation for different packing fractions η we find out the whole phase diagram of RLIF in the η-βV_0 plane.

Small, residual numerical errors in x_0' and y_0' translate into errors in the location of the phase transition points. These are calculated as follows. The quantity βK_{xy} varies linearly with η at all potential strengths. Therefore the numerical error in η is proportional to the error in βK_{xy} (see Fig. 13). The error in y_0' is neglected [56]. The final error estimates are shown (as vertical error bars) in our results for the phase diagram of hard disks in an external potential in Fig. 12.

Compared with previous computations [28,29] of the phase diagram for this system (also shown in Fig. 12) we find that, within error bars, our results agree at all values of η and βV_0 with the results of Strepp *et al.* [29]. In numerical details, they, however, disagree with the results of Das *et al.* [28], though even these results show RLIF and are in quali-

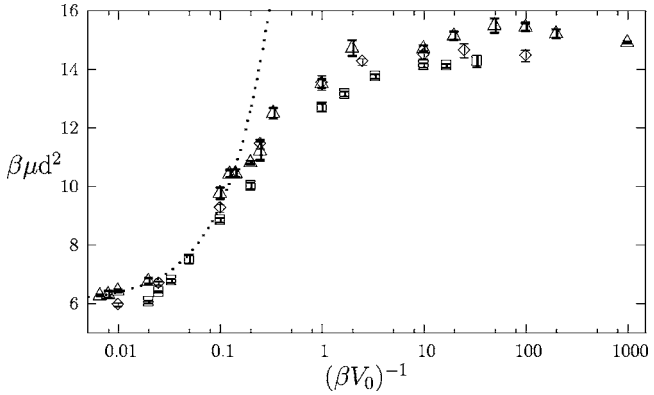

FIG. 10. Shear modulus $\beta\mu d^2$ as a function of inverse laser potential $(\beta V_0)^{-1}$. Various symbols denote different densities: ◇ denotes $\eta=0.7029$, ◇ denotes $\eta=0.705$, and □ denotes $\eta=0.7$. The dotted line is a linear fit of the form $\beta\mu d^2=a/\beta V_0+b$ in the large-βV_0 limit [36].

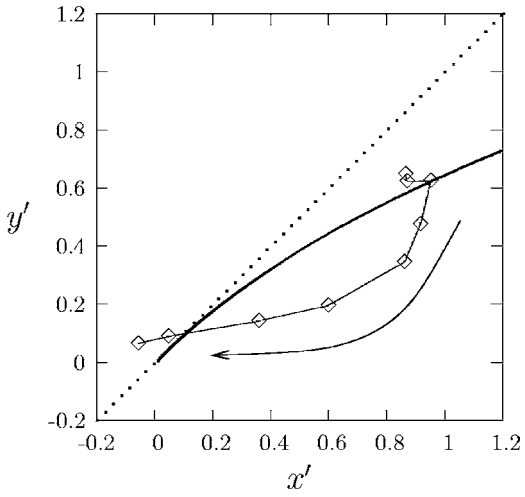

FIG. 11. The initial values of x' and y' obtained from the elastic moduli and dislocation probability at $\eta=0.7029$ plotted in the x'-y' plane. The line connecting the points is a guide to the eye. The arrow shows the direction of increase in βV_0 (=0.01,0.04,0.1, 0.4,1,4,10,40,100). The dotted line denotes the separatrix ($y'=x'$) incorporating only the leading order term in the KT flow equations. The solid curve is the separatrix when next to leading order terms are included. In the $l\to\infty$ limit any initial value below the separatrix flows to the $y'=0$ line whereas that above the separatrix flows to $y'\to\infty$. The intersection points of the line of initial values with the separatrix give the phase transition points. The plot shows a freezing transition at $\beta V_0=0.1$ followed by a melting at $\beta V_0=30$.

tative agreement with ours. This validates both our method and the quantitative predictions of Refs. [35,36].

The effect of higher-order terms in determining nonuniversal quantities has been pointed out earlier [6] for the planar rotor model but in the present case their inclusion appears to be crucial. Nevertheless, we expect our procedure to break down in the $\beta V_0\to 0$ limit where effects due to the crossover from a KT to a KTHNY [8,9] transition at $\beta V_0=0$ become significant. Indeed, as is evident from Fig. 3 for $\beta V_0<1$ the dislocation probabilities of both type I and type II dislocations are similar [57] and the assumptions of FNR theory and our process (which involves only type I dislocations) need not be valid at small potential strengths. This fact is also supported by Ref. [29] where it was shown that though at $\beta V_0=1000$ the scaling of susceptibility and order parameter cumulants gave good data collapse with values of critical exponents close to FNR predictions, at $\beta V_0=0.5$, on the other hand, ordinary critical scaling gave better data collapse than the KT scaling form, perhaps due to the above mentioned crossover effects. In the asymptotic limit of $\beta V_0\to\infty$ the system freezes above $\eta=0.706$ which was determined from a separate simulation in that limit. This number is very close to the earlier value $\eta\sim 0.71$ quoted in Ref. [29]. As expected, the freezing density in the $\beta V_0\to\infty$ limit is lower than the value without the periodic potential, i.e., $\eta\simeq 0.715$.

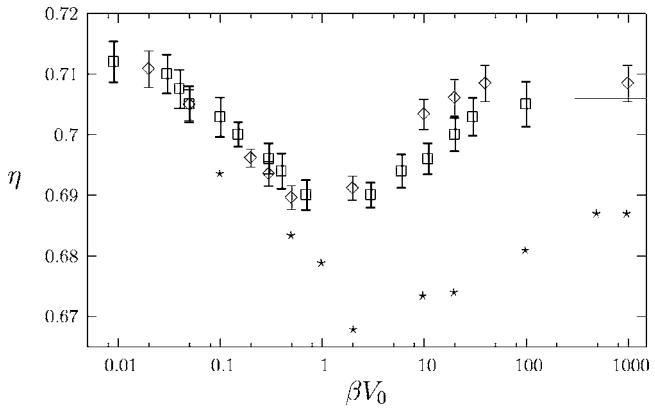

FIG. 12. The phase diagram of the hard disk system in the presence of a 1D, commensurate, periodic potential in the packing fraction (η)–potential strength (βV_0) plane. The points denoted by $\square$ correspond to our RG calculation using the techniques described in this paper. The points denoted by $\diamond$ [29] and * [28] are taken from earlier simulations. The vertical bars denote estimate of error. Our data clearly match with Ref. [7]. The horizontal line at $\eta=0.706$ denotes the calculated asymptotic phase transition point at $\beta V_0=\infty$.

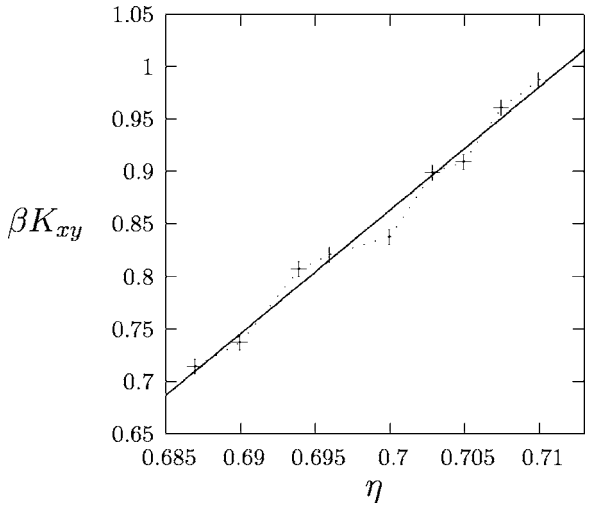

FIG. 13. For the hard disk system $\tilde{K}_{xy}=\beta K_{xy}$ varies linearly with η. Data plotted at $V_0=1$. The solid line is a linear fit to the form $f(x)=a+bx$ with $a=-7.37$ and $b=11.76$. At each V_0 the error in $\tilde{K}_{xy}$ determines the error in η: $\delta\eta/\eta=|1+a/\eta b|(\delta\tilde{K}_{xy}/\tilde{K}_{xy})$.

Before we go on to discuss other systems, we discuss the reasons behind the particular choice of r_{min} that we made throughout this work. After a disclination quartet is formed, they get separated out and the easy direction of separation is the glide direction which is parallel to the Burgers vector. In Fig. 14 we show four steps of separation of such a dislocation pair of type I. It is clear that it is possible to give individual identification to a dislocation only when the Burgers vector separation within a pair is $\geqslant 2a_0$ (Fig. 14), i.e., $r_{min}=2a_0$. For $r\geqslant 2a_0$ Burgers loops can be drawn around each 5-7 disclination pair (Fig. 14) giving rise to a nonzero Burgers vector. After motivating $r_{min}=2a_0$ we show, in Fig. 15, the three sets of initial values corresponding to $r_{min}=a_0,2a_0,3a_0$ along with the nonlinear separatrix at $\eta=0.7029$ of a hard disk system. It is clear from the figure that $r_{min}=a_0$ predicts the system to be in the solid phase for any

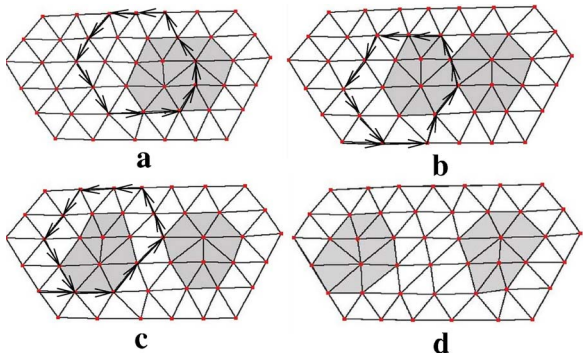

FIG. 14. (Color online) (a)–(d), which we have drawn using the applet "voroglide" [58], show four steps of separation of a type I dislocation pair, from a separation of a_0 to $4a_0$. The shaded regions show the 5-7 disclination pairs constituting the dislocations. Burgers circuits are shown in (a)–(c). Note that for separations $\geqslant 2a_0$ separate Burgers circuits around each disclination pair give rise to nonzero Burgers vectors, giving the dislocations their individual identity. This shows that the minimum meaningful separation between dislocation cores $r_{min}=2a_0$.

arbitrarily small amount of external potential and to melt at larger βV_0. This behavior contradicts the physical expectation that the melting density at $\beta V_0=0$ has to be larger than that at $\beta V_0=\infty$. On the other hand, while $r_{min}=3a_0$ does not produce any unphysical prediction, it shrinks the region of reentrance in the βV_0 direction. It is therefore satisfying to note that $r_{min}=2a_0$, the minimum possible value for the separation between members of a dislocation-antidislocation pair which allows unambiguous identification also produces physically meaningful results for the phase diagram, in closest agreement with earlier simulation data.

It is possible to find out phase diagrams of any 2D system in the presence of an external modulating potential commensurate with the density of the system in a similar fashion. We illustrate this by calculating similar phase diagrams for two other systems, viz., soft disks and the DLVO system.

B. Soft disks

Soft disks interact via the potential

$$\phi(r) = \frac{1}{r^{12}}$$

where r denotes the separation between particles. In simulations, the cutoff distance is chosen to be $r_c=2$ above which the particles are assumed to be noninteracting. Apart from the external potential strength βV_0 the relevant thermodynamic quantity is the number density $\rho=N/L_xL_y$. To obtain bare elastic moduli from restricted simulations the stress is calculated using Eq. (7). As this expression does not involve any Dirac δ functions (unlike hard disks), we do not require any fitting and extrapolation to obtain the stresses and the errors are purely due to random statistical fluctuations in our MC simulations. The elastic moduli are again found from stress-strain curves like Figs. 7 and 8. The dislocation fugacity of type I is calculated from the rejection ratio of dislocation-generating moves. All these, at a given ρ value

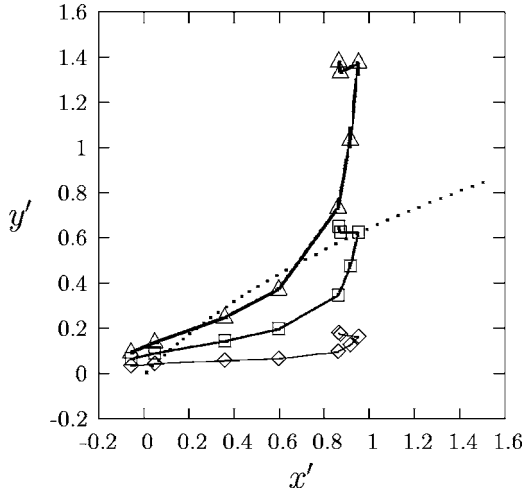

FIG. 15. Similar to Fig. 11. The initial conditions x_0' and y_0' are plotted as a function of βV_0. The different data sets are created for different values of r_{min}. The symbols mean the following: ◇ denote data for $r_{min}=a_0$, □ denote those for $r_{min}=2a_0$, and △ denote data for $r_{min}=3a_0$. The dotted line denotes the nonlinear separatrix.

generate the initial conditions x_0' and y_0' in RG flow diagrams. Again, the crossing of these initial conditions with the separatrix found from Eq. (2) gives the phase transition points. The phase diagram is plotted and compared with the phase diagram from earlier simulations [31,32] in Fig. 16. The error bar in ρ is found from the error in $\tilde{K}_{xy}$, as $\tilde{K}_{xy}$ varies linearly with ρ, through the relation $\delta\rho/\rho=|1+a/\rho b|(\delta\tilde{K}_{xy}/\tilde{K}_{xy})$ where a and b are obtained from a linear $(a+bx)$ fit of the $\tilde{K}_{xy}$ vs ρ curve, at any given βV_0. The phase diagram (Fig. 16) again clearly shows reentrance (RLIF). This is in qualitative agreement with earlier simulations [31,32] (see Fig. 16).

C. DLVO

For charge-stabilized colloids the interparticle potential that operates is approximately given by the DLVO potential [47,48]:

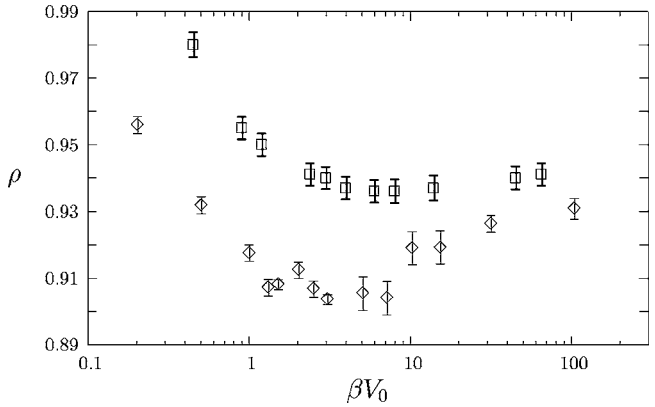

FIG. 16. Phase diagram for soft disks: □ denote our calculation, ◇ indicate earlier simulation data [31,32]. The vertical lines are the error bars.

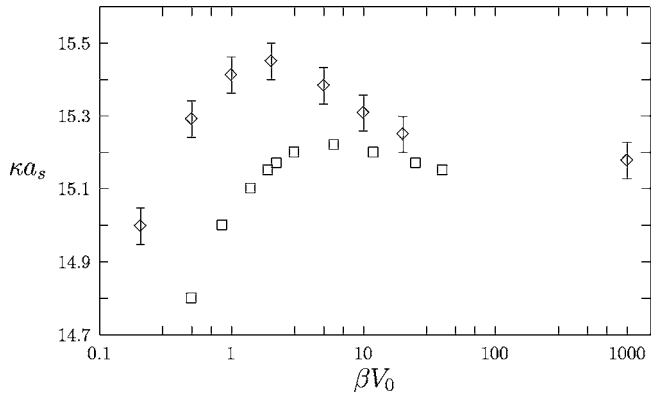

FIG. 17. Phase diagram for particles interacting via the DLVO potential. □ denote our calculation; ◇ show the earlier simulation data [30]. The vertical lines are the error bars. Error bars in our calculation, being smaller than the symbol size, are not shown.

$$\phi(r) = \frac{(Z^* e)^2}{4\pi\epsilon_0\epsilon_r}\left(\frac{\exp(0.5\kappa d)}{1+0.5\kappa d}\right)^2 \frac{\exp(-\kappa r)}{r}$$

where r is the separation between two particles, d is the diameter of the colloids, κ is the inverse Debye screening length, Z^* is the amount of effective surface charge, and ϵ_r is the dielectric constant of the water in which the colloids are floating. In order to remain close to experimental situations and to be able to compare our phase diagram with the simulations of Strepp *et al.* [29] we use $T=293.15$ K, $d=1.07$ μm, $Z^*=7800$, $\epsilon_r=78$. In experiments, the dimensionless inverse Debye screening length κa_s can be varied either by changing κ through the change in counterion concentration or by changing a_s by varying density [59]. In our restricted MC simulations we vary κ keeping the density fixed at 0.18 μm^{-2} by fixing the lattice parameter of the initial configuration of an ideal triangular lattice at $a_s=2.525\,78$ μm. Further, we use a cutoff radius r_c such that $\phi(r>r_c)=0$ where r_c is found from the condition $\beta\phi(r_c)=0.001$. We find out phase transition points (in κa_s) at different external potential strengths βV_0 in the same fashion as described earlier. The phase diagram in the $\kappa a_s - \beta V_0$ plane is shown in Fig. 17. To obtain error bars in this case we note that $\tilde{K}_{xy}$ varies linearly with κa_s and therefore the error in $\tilde{K}_{xy}$ is proportional to the error in κa_s (Fig. 17) through the relation $\delta(\kappa a_s)/(\kappa a_s) = |1 + a/b\kappa a_s|(\delta\tilde{K}_{xy}/\tilde{K}_{xy})$. The quantities a and b are found from fitting $\tilde{K}_{xy}$ to a linear form of κa_s, at any given βV_0.

Though there is a quantitative mismatch between our data and those of Strepp *et al.* [30], our data show a clear region in κa_s (between 15.1 and 15.2) where we obtain reentrance (RLIF). This is in contrast to the simulated phase diagram of Das *et al.* [28], where they observe absence of reentrance at high field strengths. We do not plot their data as the parameters these authors used are not the same as the ones used in Fig. 17.

It is interesting to note that, with increase in the range of the two-body interaction potentials the depth of reentrance (in η, ρ, or κa_s) decreases. This is again in agreement with the understanding that the reentrant melting comes about due to decoupling of the 1D trapped layers of particles which reduces the effective dimensionality, thereby increasing fluctuations. With an increase in range of the interacting potentials this decoupling gets more and more suppressed, thereby reducing the region of reentrance.

One aspect of our study which stands out is the exceptionally better agreement of our results with previous simulations for hard disks as opposed to systems with soft potentials like the soft disks and the DLVO. This could, in principle, be due either (a) to the failure of the RG equations used by us or some other assumptions in our calculations or (b) to unaccounted-for finite size effects in earlier simulations. While it is difficult to estimate the effect of (a) since RG equations to higher orders in y are unknown at present, we may be able to motivate an estimation for (b). In order to explain the discrepancy in the positions of the phase boundaries, we need to go into some detail of how the phase diagrams were obtained in the earlier simulations. In these simulations [29–32] the phase boundaries were obtained from the crossing of the order parameter cumulants [38,39] for various coarse graining sizes. The system sizes simulated in these studies are the same ($N=1024$). However, the range of interaction differs. To obtain an objective measure we define the range of the potentials ξ as that at which the interaction potential ϕ is only 1% of its value at the lattice parameter. In units of lattice parameter, we obtain for soft disks $\xi=1.47$ and for the DLVO potential $\xi=1.29$ at typical screening of $\kappa a_s=15$. By definition, for hard disks $\xi=1$. The particles within the range of the potential are highly correlated and we calculate the number N_{corr} of such independent bare *uncorrelated particles* within the full system size. N_{corr} takes the values $N_{corr}=1024$, 473.88, and 615.35 for hard disks, soft disks, and the DLVO potential, respectively. Since the effective system sizes are smaller for the soft potentials, finite size effects are expected to be larger. In this connection, it is of interest to note that in the same publications [29–32] a systematic finite size analysis showed that the phase diagrams shift toward higher (lower) density (κ) for hard and soft disks (DLVO). A look at Figs. 16 and 17 should convince the reader that such a shift would actually make the agreement with our results better. We emphasize here that our present restricted simulations are virtually free of finite size effects since the system does not undergo any phase transition.

IV. CONCLUSION

We have presented a complete numerical renormalization group scheme to calculate phase diagrams for 2D systems under a commensurate modulating potential. We have used FNR theory along with this scheme to calculate phase diagrams for three different systems, namely, the hard disks, the DLVO potential, and the soft disks. In all the cases we have found laser-induced freezing followed by a reentrant laser-induced melting. We show that the reentrance behavior is built into the bare quantities themselves. We find extremely good agreement with earlier simulation results. In particular the phase diagram for hard disk comes out to be exactly the

same as found from one set of earlier simulations [29]. To obtain the correct phase diagram, however, flow equations need to be correct at least up to next to leading order terms in the dislocation fugacity. Our results, especially for small potential strengths, is particularly sensitive to these terms. Crossover effects from the zero-potential KTHNY melting transition are also substantial at small values of the potential.

ACKNOWLEDGMENTS

The authors thank Peter Nielaba, Wolfram Strepp, Abhishek Chaudhuri, Erwin Frey, Abhishek Dhar, Madan Rao, and Yacov Kantor for useful discussions; D.C. thanks CSIR, India, for financial support. Financial support by DST Grant No. SP/S2/M-20/2001 is gratefully acknowledged.

[1] J. M. Kosterlitz and D. J. Thouless, J. Phys. C **6**, 1181 (1973).
[2] J. Tobochnik and G. V. Chester, Phys. Rev. B **20**, 3761 (1979).
[3] J. F. Fernández, M. F. Ferreira, and J. Stankiewicz, Phys. Rev. B **34**, 292 (1986).
[4] R. Gupta, J. DeLapp, G. G. Batrouni, G. C. Fox, C. F. Baillie, and J. Apostolakis, Phys. Rev. Lett. **61**, 1996 (1988).
[5] P. Minnhagen, Rev. Mod. Phys. **59**, 1001 (1987).
[6] S. Sengupta, P. Nielaba, and K. Binder, Europhys. Lett. **50**, 668 (2000).
[7] R. H. Morf, Phys. Rev. Lett. **43**, 931 (1979).
[8] D. R. Nelson and B. I. Halperin, Phys. Rev. B **19**, 2457 (1979).
[9] A. P. Young, Phys. Rev. B **19**, 1855 (1979).
[10] K. J. Strandburg, Rev. Mod. Phys. **60**, 161 (1988).
[11] S. Sengupta, P. Nielaba, and K. Binder, Phys. Rev. E **61**, 6294 (2000).
[12] M. S. Rzchowski, S. P. Benz, M. Tinkham, and C. J. Lobb, Phys. Rev. B **42**, 2041 (1990).
[13] S. N. Coppersmith *et al.*, Phys. Rev. Lett. **46**, 549 (1981).
[14] A. Chowdhury, B. J. Ackerson, and N. A. Clark, Phys. Rev. Lett. **55**, 833 (1985).
[15] Q.-H. Wei, C. Bechinger, D. Rudhardt, and P. Leiderer, Phys. Rev. Lett. **81**, 2606 (1998).
[16] F. Huang, M. T. Kief, G. J. Mankey, and R. F. Willis, Phys. Rev. B **49**, 3962 (1994).
[17] W. Dürr *et al.*, Phys. Rev. Lett. **62**, 206 (1989).
[18] *Ordering in Two Dimensions*, edited by S. K. Sinha (North-Holland, Amsterdam, 1980).
[19] K. J. Strandburg, Phys. Rev. B **34**, 3536 (1986).
[20] D. R. Nelson, in *Phase Transitions and Critical Phenomena*, edited by C. Domb and J. Lebowitz (Academic Press, New York, 1983), Vol. 7, p. 1.
[21] M. S. S. Challa and D. P. Landau, Phys. Rev. B **33**, 437 (1986).
[22] A. Zippelius, B. I. Halperin, and D. R. Nelson, Phys. Rev. B **22**, 2514 (1980).
[23] D. Chaudhuri and S. Sengupta, Europhys. Lett. **67**, 814 (2004).
[24] D. Chaudhuri and S. Sengupta, Europhys. Lett. **68**, 160 (2004).
[25] J. Chakrabarti, H. R. Krishnamurthy, A. K. Sood, and S. Sengupta, Phys. Rev. Lett. **75**, 2232 (1995).
[26] C. Das and H. R. Krishnamurthy, Phys. Rev. B **58**, R5889 (1998).
[27] C. Das, A. K. Sood, and H. R. Krishnamurthy, Physica A **270**, 237 (1999).
[28] C. Das, P. Chaudhuri, A. K. Sood, and H. R. Krishnamurthy, Curr. Sci. **80**, 959 (2001).
[29] W. Strepp, S. Sengupta, and P. Nielaba, Phys. Rev. E **63**, 046106 (2001).
[30] W. Strepp, S. Sengupta, and P. Nielaba, Phys. Rev. E **66**, 056109 (2002).
[31] W. Strepp, S. Sengupta, M. Lohrer, and P. Nielaba, Comput. Phys. Commun. **147**, 370 (2002).
[32] W. Strepp, S. Sengupta, M. Lohrer, and P. Nielaba, Math. Comput. Simul. **62**, 519 (2003).
[33] Pinaki Chaudhuri, Chinmoy Das, Chandan Dasgupta, H. R. Krishnamurthy, and A. K. Sood, Phys. Rev. E **72**, 061404 (2005).
[34] J. Chakrabarti, H. R. Krishnamurthy, and A. K. Sood, Phys. Rev. Lett. **73**, 2923 (1994).
[35] E. Frey, D. R. Nelson, and L. Radzihovsky, Phys. Rev. Lett. **83**, 2977 (1999).
[36] L. Radzihovsky, E. Frey, and D. R. Nelson, Phys. Rev. E **63**, 031503 (2000).
[37] I. W. Hamley, *Introduction to Soft Matter: Polymer, Colloids, Amphiphiles and Liquid Crystals* (Wiley, Chichester, U.K., 2000).
[38] K. Binder, Phys. Rev. Lett. **47**, 693 (1981).
[39] D. P. Landau and K. Binder, *A Guide to Monte Carlo Simulations in Statistical Physics* (Cambridge University Press, Cambridge, U.K., 2000).
[40] D. S. Fisher, B. I. Halperin, and R. Morf, Phys. Rev. B **20**, 4692 (1979).
[41] A. Jaster, Physica A **277**, 106 (2000).
[42] D. J. Amit, Y. Y. Goldschmidt, and G. Grinstein, J. Phys. A **13**, 585 (1980).
[43] This assumption is similar in spirit to assuming that a particle which reaches the saddle point in the Kramers barrier crossing problem would automatically cross the barrier [H. A. Kramers, Physica (Amsterdam) **7**, 284 (1940)].
[44] Note that the calculation of the bare fugacity from the dislocation probability is, we believe, more accurate than the procedure used in [23].
[45] O. Farago and Y. Kantor, Phys. Rev. E **61**, 2478 (2000).
[46] In the presence of an external 1D modulating potential periodic in the y direction the stress has contribution from another virial-like additive term $(-\beta d^2/S)\langle\Sigma_\lambda y^\lambda f_y^\lambda\rangle$, where y^λ is the y component of the position vector of particle λ. This contribution comes from the part of the free energy that involves higher-energy (massive) excitations. For the elastic free energy which is lowest order in the displacement gradient [Eq. (1)] this part does not contribute toward the elastic constants, as the x and y components of gradient remain uncoupled. This extra term in stress remains a constant background without disturbing the elastic constants connected to the Young and shear

moduli which corresponds to distortions of the system in the low-energy directions. We therefore neglect this background in calculating stresses wherefrom we obtain the elastic moduli.

[47] E. J. W. Verwey and J. T. G. Overbeek, *Theory of Stability of Lyophobic Colloids* (Elsevier, Amsterdam, 1948).

[48] B. V. Derjaguin, and L. D. Landau, Acta Physicochim. URSS **14**, 633 (1941).

[49] B. Alder and T. Wainwright, Phys. Rev. **127**, 359 (1962).

[50] J. A. Zollweg, G. V. Chester, and P. W. Leung, Phys. Rev. B **39**, 9518 (1989).

[51] H. Weber and D. Marx, Europhys. Lett. **27**, 593 (1994).

[52] V. N. Ryzhov and E. E. Tareyeva, Phys. Rev. B **51**, 8789 (1995).

[53] J. P. Hansen and I. R. MacDonald, *Theory of Simple Liquids* (Wiley, Chichester, U.K., 1989).

[54] This interaction in colloids is due to polarization of the dielectric colloidal particles by the electric field of the laser. Though the experiments of Refs. [14,15] use charged colloids, the interaction of hard sphere colloids with lasers is similar.

[55] D. Frenkel and B. Smit, *Understanding Molecular Simulation*, 2nd ed. (Academic Press, New York, 2002).

[56] The error in y_0' has contributions from both P_{di}s and from K_{xy}; while the former is practically zero, the contribution from the latter is neglected in this work.

[57] In analyzing Fig. 3 we must keep in mind that we can calculate from our simulations only the probability of formation of a disclination quartet. While we can, perhaps, safely assume that if type I dislocations are involved, they will separate out with unit probability, the same cannot be said of type II dislocations. This means that the probability of type II dislocations could be much lower than what Fig. 3 suggests.

[58] http://www.pi6.fernuni-hagen.de/GeomLab/VoroGlide/index.html.en

[59] C. Bechinger and E. Frey, J. Phys.: Condens. Matter **13**, R321 (2001).